

Vacancy effects in an easy-plane Heisenberg model: reduction of T_c and doubly-charged vortices

G. M. Wysin*

Departamento de Física, Universidade Federal de Viçosa, Viçosa, 36570-000, Minas Gerais, Brazil †

(Dated: November 8, 2004)

Magnetic vortices in thermal equilibrium in two-dimensional magnets are studied here under the presence of a low concentration of nonmagnetic impurities (spin vacancies). A nearest-neighbor Heisenberg (XXZ) spin model with easy-plane exchange anisotropy is used to determine static thermodynamic properties and vortex densities via cluster/over-relaxation Monte Carlo. Especially at low temperature, a large fraction of the thermally generated vortices nucleate centered on vacancies, where they have a lower energy of formation. These facts are responsible for the reduction of the vortex-unbinding transition temperature with increasing vacancy concentration, similar to that seen in the planar rotator model. Spin vacancies also present the possibility of a new effect, namely, the appearance of vortices with double topological charges ($\pm 4\pi$ change in in-plane spin angle), stable only when centered on vacancies.

PACS numbers: 75.10Hk, 75.30Ds, 75.40Gb, 75.40Mg

I. INTRODUCTION

The vortex-unbinding transition in two-dimensional (2D) spin models with planar symmetry (Berezinskii-Kosterlitz-Thouless transition^{1,2,3}) has attracted interest recently with respect to the influence of nonmagnetic impurities or spin vacancies in the lattice. In any real physical system, some fraction of the atoms could be substituted by impurities, and if these are nonmagnetic, the spins neighboring the impurity will be strongly affected by the missing exchange interactions. Not only could missing bonds cause locally lower energy densities, but they give the neighboring spins more freedom of motion, which can be expected to increase the local spin fluctuations. This can be expected to affect the static configurations, the thermal equilibrium properties, and the dynamic correlations, such as in EPR measurements on antiferromagnets.^{4,5}

Significant vacancy effects on the static vortex (or antivortex) configurations of ferromagnets (and antiferromagnets with two sublattices) have already been found for a 2D easy-plane Heisenberg model (three spin components). Zaspel *et al.*⁶ found that the critical anisotropy strength ($\delta_c \equiv 1 - \lambda_c$, see Hamiltonian below) needed to stabilize a vortex in the planar configuration on a square lattice is reduced from $\delta_c \approx 0.2966$ to the much lower value $\delta_{cv} \approx 0.0429$ when the vortex is centered on a vacancy. Wysin⁷ found a similar result at higher precision ($\delta_{cv} \approx 0.0455$), and determined that a vacancy at the center of a circular system with free boundaries produces an attractive potential for a vortex. Using dynamic relaxation and Monte Carlo simulations, Pereira *et al.*⁸ found that a single vacancy in a square system with antiperiodic boundary conditions provides an attractive potential for a vortex. These works demonstrated a significant energy reduction for a vortex formed on a vacancy, compared to one formed in the center of a cell of the lattice, whose value depends on the type of lattice and the boundary conditions. The resulting vortex-on-vacancy binding

energy was found to increase with increasing easy-plane anisotropy strength. Both analytic and numerical calculations by Paula *et al.*⁹ show that holes cut out of a spin lattice similarly produce interesting attractive effects on vortices.

Continuum model calculations for the closely related planar rotator model^{10,11} were interpreted to suggest a repulsive potential between a planar vortex and a nonmagnetic impurity, however, this seems contradictory to later calculations. Studies of a 2D isotropic Heisenberg antiferromagnet by Mól *et al.*¹² and Pereira and Pires¹³ found oscillatory dynamic modes of solitons pinned to vacancies, confirming the presence of an attractive restoring potential. Considering these most recent calculations for several models,^{7,8,9,12,13} in general it has been seen that a spin vacancy attracts vortices (or antivortices) and lowers their energy of formation.

In terms of the equilibrium thermodynamics, the effect of a concentration of vacancies on the BKT transition temperature T_c of the easy-plane Heisenberg model has not been studied. On the other hand, Leonel *et al.*¹¹ performed Monte Carlo (MC) simulations of the planar rotator model (two-component spins) and found a lowering of the transition temperature with increasing vacancy density. It was argued that vacancies produce an effective repulsive potential for vortices, thereby increasing the nucleation of pairs and lowering the transition temperature, but the vortex density was not measured in the MC simulations. Using the helicity modulus to determine T_c , they found that T_c goes to zero when the vacancy concentration of a square lattice reaches about 30%. A similar lowering of T_c also appears in the MC simulations of Berche *et al.*¹⁴ for the same model, determined by fitting the exponent of the spin-spin correlation function to the critical point value, $\eta = 1/4$. These latter authors found that T_c did not fall to zero until the vacancy concentration reached 41%, a number related to the percolation threshold for a square lattice. In a related bond-diluted planar rotator model, Castro *et al.*¹⁵ used a

self-consistent harmonic approximation with vortex corrections, determining the reduction of T_c with dilution, and the temperature variation of the correlation function and its exponent η .

Here it is interesting to consider whether a similar vacancy-induced reduction of T_c occurs in the anisotropic Heisenberg model, which is a more realistic spin model that has a true time dynamics. An analysis of the vortex densities in thermal equilibrium, in the presence of vacancies, helps to explain the role of vacancies in generating spin disorder around the transition temperature. The vortices in the anisotropic Heisenberg model also can be expected to have planar or out-of-plane structure, depending on the anisotropy strength.^{16,17,18,19,20,21,22} At stronger anisotropy [i.e., for the XY model, $\lambda = 0$, see Eq. (1)], the stable static vortices are planar, whether pinned on vacancies or free from the vacancies.^{6,7} Alternatively, at weak anisotropy, both the stable pinned and free vortices have nonzero out-of-plane spin components, which might be expected to significantly modify some equilibrium properties as well as dynamic correlations. Therefore, here we present MC simulations for three different anisotropies, calculating the changes in T_c and the behavior of the vortex densities, as well as other thermodynamic properties.

It has been customary only to search for singly charged vortices appearing in MC simulations of pure easy-plane spin systems. Looking in individual unit cells (plaquettes) of the lattice, a net rotation of the in-plane spin angles through $\pm 2\pi$ as one moves around the cell indicates the presence of a singly-charged vortex ($q = \pm 1$). When vacancies are present, however, the searching for vorticity must be modified. Here, we searched for net vorticity also in the four unit cells surrounding any vacancy of the square lattice. This allows for the appearance of a new effect, namely, the presence of $q = \pm 2$ vortices, which always form centered on the vacancies. They appear as a very small fraction of the total vorticity density, and are present regardless of the anisotropy strength. Apparently, by pinning on vacancies, $q = \pm 2$ vortices lower their energy sufficiently due to the missing spin site, leading to greater ease in their thermal formation. In addition, at low temperatures, it is found that most vortices (either $q = \pm 1$ or $q = \pm 2$) form initially on the vacancies, which gives an interesting view of how vacancies modify and even control the BKT transition.

After further definition of the model, we describe the MC simulations, determinations of T_c using finite-size scaling of the in-plane susceptibility, and the vacancy effects at various anisotropies. This is followed by some preliminary analysis of the stability properties of the doubly-charged vortices.

II. EASY-PLANE MODEL WITH RANDOM REPULSIVE VACANCIES

The model to be investigated has classical three-component spins defined at the sites \mathbf{n} of a 2D square lattice with unit lattice constant. The spins can be analyzed either in terms of their Cartesian components or using polar spherical coordinate angles, $\vec{S} = (S^x, S^y, S^z) = S(\sin\theta \cos\phi, \sin\theta \sin\phi, \cos\theta)$. The system is an $L \times L$ square with periodic boundary conditions. We considered L ranging from 16 to 128, using the dependence of the thermodynamic averages on L to get estimates of the critical temperature in the infinite size system.

A small vacancy density ρ_{vac} is introduced into the lattice as follows. An occupation number $p_{\mathbf{n}}$ for each site is set to the static values 1 or 0 depending on whether the site \mathbf{n} is occupied by a spin or is vacant. The fraction ρ_{vac} of the sites has $p_{\mathbf{n}}$ set to zero. (Equivalently, one can keep the spins at the vacant sites but set their lengths to zero.) In order to have the most simplified situation, the vacant sites are chosen randomly, but no two are allowed to be within the second nearest neighbor distance of $\sqrt{2}$ (the diagonal separation across a unit cell of the lattice). In this way, the immediate neighborhoods of all vacancies are equivalent: each vacant site is surrounded by eight occupied sites. This condition greatly simplifies the algorithm for searching for localized vorticity around the vacant sites. On the other hand, it limits the possible density of vacancies to be less than 0.25 of the lattice sites (achieved in the ordered configuration having alternating rows of the lattice fully and half occupied by spins). In actual practice, by choosing the vacant sites randomly and enforcing this constraint (i.e., quenched repulsive vacancies), the maximum achievable vacancy density is $\rho_{\text{vac}} \approx 0.1872$. As a result, a vacancy density needed to push the BKT transition temperature down to zero cannot be achieved, and we do not consider this aspect of the model here. Instead, we are more interested in the role the vacancies play in controlling where the vortices are forming.

Nearest neighbor unit length spins ($S = 1$) in this model interact ferromagnetically (exchange constant $J > 0$) according to a Hamiltonian with easy-plane anisotropy specified by parameter λ ,

$$H = \frac{-J}{2} \sum_{\mathbf{n}, \mathbf{a}} p_{\mathbf{n}} p_{\mathbf{n}+\mathbf{a}} \left[S_{\mathbf{n}}^x S_{\mathbf{n}+\mathbf{a}}^x + S_{\mathbf{n}}^y S_{\mathbf{n}+\mathbf{a}}^y + \lambda S_{\mathbf{n}}^z S_{\mathbf{n}+\mathbf{a}}^z \right]. \quad (1)$$

The XY-model results for $\lambda = 0$. Values of λ below 1 describe a system where z is the hard axis and xy is the easy plane, allowing for the appearance of vortices. The total number of spins in the system is

$$N = N_{\text{occ}} = (1 - \rho_{\text{vac}})L^2. \quad (2)$$

In general, calculated thermodynamic quantities are quoted here as per-occupied-site average values, i.e., normalized by N .

III. MC SIMULATIONS

Classical Monte Carlo algorithms were used to estimate static thermodynamic quantities as functions of temperature T , with emphasis on the internal energy $e = E/N$, specific heat $c = C/N$, and magnetic susceptibility of the in-plane spin components, χ , all per-occupied-site quantities, as well as the vorticity densities per occupied site. It is understood that a certain percent of vacancies ρ_{vac} has been produced in the $L \times L$ lattice under study, at randomly selected positions as described above. We found there to be very little variation in the results with the choice of equivalent systems with different vacancy positions, especially for the larger lattices (i.e., a large system is self-averaging). Therefore, no averaging over different systems at a given L was performed.

A. MC Algorithm

The MC techniques used here have been described in Ref. 23 and are based partly on simulation methods developed in Refs. 24,25,26,27. We applied a combination of Metropolis single-spin moves and over-relaxation moves²⁸ that modify all three spin components, and in addition, Wolff single-cluster operations^{29,30} that modify *only* the xy spin components. The single spin moves and over-relaxation moves were applied to sites selected randomly in the lattice; similarly, the initial sites for cluster generation were selected randomly.

In the single-spin moves, randomly selected spins were modified by adding small increments in random directions, and then renormalizing the spins to unit length, accepting or rejecting each change according to the Metropolis algorithm.

The over-relaxation and cluster moves are important at low temperatures, where the xy spin components tend to freeze and single spin moves become inefficient. Over-relaxation and cluster moves have the tendency to change spin directions with no or very small changes in energy, hence, their efficacy at low temperature.

The over-relaxation moves used here consist of reflecting a randomly selected spin across the effective magnetic field due to its neighbors,

$$\vec{B}_{\mathbf{n}} = J \sum_{\mathbf{a}} p_{\mathbf{n}+\mathbf{a}} [S_{\mathbf{n}+\mathbf{a}}^x \hat{x} + S_{\mathbf{n}+\mathbf{a}}^y \hat{y} + \lambda S_{\mathbf{n}+\mathbf{a}}^z \hat{z}], \quad (3)$$

while preserving the spin length. All spin components are involved in the process, and the z components become more greatly involved when the anisotropy parameter λ approaches 1. This spin change exactly conserves the energy, while effectively mixing up the spin directions.

The Wolff cluster algorithm (and computer subroutine) used here is identical to that used for the pure system without vacancies. In the actual computations, the spins of the vacant lattice sites are set to zero length (equivalent to setting occupation $p_{\mathbf{n}} = 0$), and the calculations proceed normally. No other significant changes

are needed to implement the Wolff algorithm. It means that the Wolff clusters being formed could actually span across vacant sites. Clearly, this means that a large cluster being formed might actually be composed from several sub-clusters connected by vacant sites, a situation that probably enhances the mixing produced by the algorithm.

For a single MC step (an MC pass through the lattice), we *attempted* N over-relaxation moves, followed by N single-spin moves, followed by N cluster moves. An initial set of 5000 MC steps was used to equilibrate the system. The averages shown here result from a sequence of 300,000 MC steps at each individual lattice size and temperature. For most of the data, the error bars are smaller than the symbols used, hence, error bars have not been displayed.

B. MC Measurements

In terms of temperature T and Boltzman's constant k , the system's thermodynamic energy E and heat capacity C are defined via usual relations,

$$E = \langle H \rangle, \quad C = k[\langle H^2 \rangle - \langle H \rangle^2]/T^2. \quad (4)$$

The instantaneous total magnetization of the system is the sum over all spins

$$\vec{M} = \sum_{\mathbf{n}} p_{\mathbf{n}} \vec{S}_{\mathbf{n}}. \quad (5)$$

For purposes of finding T_c , it is important to calculate the associated per-spin susceptibility $\chi^{\alpha\alpha}$ of any component α , derived from the magnetization fluctuations,

$$\chi^{\alpha\alpha} = (\langle M_{\alpha}^2 \rangle - \langle M_{\alpha} \rangle^2)/(NT). \quad (6)$$

Both χ^{xx} and χ^{yy} were computed by (6) and then averaged to get the in-plane susceptibility,

$$\chi = (\chi^{xx} + \chi^{yy})/2. \quad (7)$$

Finite size scaling of χ was found to be the best method to determine T_c precisely, see below.

In the thermodynamic limit, according to the Mermin-Wagner theorem, $\langle \vec{M} \rangle \rightarrow 0$ at any temperature, and this holds in an approximate sense in the MC averages of finite systems. Therefore it is also interesting to calculate the system's total in-plane absolute valued magnetic moment (order parameter M^*), which only tends to zero in the high-temperature phase, and its associated per-spin susceptibility χ^* ,

$$M^* = \langle \sqrt{M_x^2 + M_y^2} \rangle, \quad \chi^* = [\langle M_x^2 + M_y^2 \rangle - M^{*2}]/(NT). \quad (8)$$

Related per-spin energy, specific heat, and order parameter (e, c, m^*), are obtained by dividing each by the number of occupied sites, N .

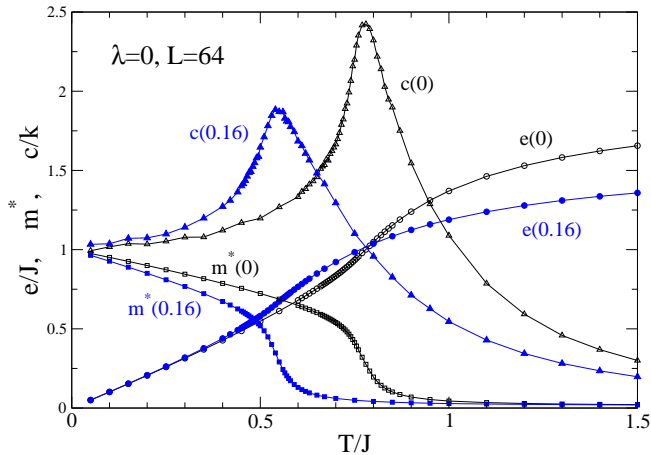


FIG. 1: For the model with edge $L = 64$, at the XY limit, the internal energy, absolute magnetization, and specific heat per spin for the uniform system and with 16% vacancy density.

For example, at $\lambda = 0$, $L = 64$, typical results for the energy, absolute in-plane magnetization and specific heat per spin are shown in Fig. 1, comparing the pure system with that at 16% vacancy concentration. Note that the energy and specific heat per spin have rather weak dependence on the system size L , while m^* acquires a sharper dropoff with increasing L . The most obvious effect of $\rho_{\text{vac}} > 0$ is the lowering of the BKT transition temperature. A less obvious effect is the lowering of the per-spin energy and specific heat in the high-temperature phase. This quite possibly results because a large fraction of the vortices produced in the high-temperature disordered phase are localized on the vacancies, as found below. When thus formed, vortices require a lower nucleation energy, and the system can reach a specified entropy at a lower overall energy cost.

C. Critical Temperature

Initially, the fourth order in-plane magnetization cumulant U_L due to Binder^{31,32} was calculated to aid in location of the transition temperature in the thermodynamic limit. It is defined using a ratio,

$$U_L = 1 - \frac{\langle (M_x^2 + M_y^2)^2 \rangle}{2\langle M_x^2 + M_y^2 \rangle^2}. \quad (9)$$

This quantity becomes 0.5 in the low-temperature ordered limit, and tends towards zero in the disordered high-temperature limit. When measured at the critical temperature, its value is expected to be approximately independent of the system size. Therefore, T_c can be estimated by plotting U_L vs. T for different system sizes and observing the common crossing point of the data. This definition of U_L is analogous to the more familiar form that would be applied to a single in-plane spin com-

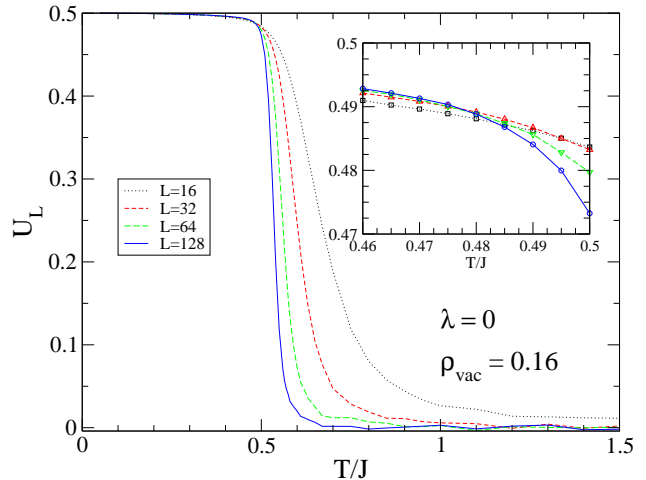


FIG. 2: Application of the L -dependence of the fourth order cumulant U_L on various system sizes to estimate $T_c/J \approx 0.48$ (common crossing point of the data) at 16% vacancy density in the XY model.

ponent or single-component model, viz.,

$$U_L^{(x)} = 1 - \frac{\langle M_x^4 \rangle}{3\langle M_x^2 \rangle^2}. \quad (10)$$

Example application of U_L for finding T_c for the XY model at 16% vacancy concentration is shown in Fig. 2. The transition temperature is lowered to $T_c \approx 0.48J$, considerably less than $T_c \approx 0.70J$ that holds at zero vacancy concentration.

It is seen, however, that U_L requires an excessive amount of calculations even to get two-digit precision for T_c . Following Cuccoli *et al.*³³ and their analysis of the pure XXZ model, a finite scaling analysis of the in-plane susceptibility χ is seen to be much more precise and efficient for finding T_c . The essential feature needed here is that near and below T_c , the susceptibility scales with a power of the system size,

$$\chi \propto L^{2-\eta}, \quad (11)$$

where the exponent η describes the long distance behavior of in-plane spin correlations below T_c , see Ref. 33 for details. Importantly, at the transition temperature for the XY model, one has $\eta = 1/4$. Here we make the assumption that $\eta = 1/4$ at T_c also for the models with $\lambda > 0$ and with vacancies present. The validity of this assumption is partially tested by the quality of the scaling that it produces.

Using $\eta = 1/4$, we plotted $\chi/L^{7/4}$ versus T for the data from different system sizes, $L = 16, 32, 64, 128$ together on one graph. The common crossing point of the curves locates the critical temperature, for example, the result $T_c/J \approx 0.699 \pm 0.001$ is easily reproduced for the vacancy-free XY model. An example of this is given in Fig. 3, for $\lambda = 0$ at 16% vacancy concentration. An exceptionally tight crossing point occurs at the critical temperature,

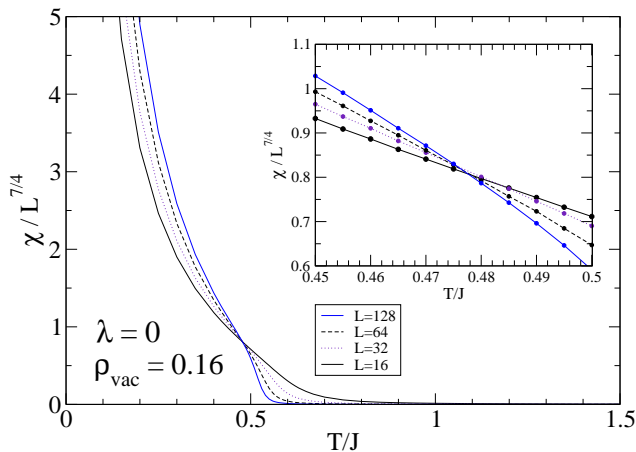


FIG. 3: Application of the finite-size scaling of in-plane susceptibility to estimate $T_c/J \approx 0.478$ (common crossing point of the data) at 16% vacancy density in the XY model, using exponent $\eta = 1/4$.

$T_c/J \approx 0.478 \pm 0.001$. The clarity of the crossing point gives considerable confidence in the $\eta = 1/4$ assumption, even when vacancies are present. Similar results hold for the other models studied (nonzero λ and nonzero ρ_{vac} , see III E) where the scaling estimates of T_c give dramatic improvement upon the more approximate estimates using U_L , from the *same* MC data.

D. Vortex densities

In a system with vacancies, the presence of unit charged and doubly charged vortices is determined as follows.

If a unit cell or plaquette is found to be fully occupied by spins, then the vortex search takes place in the usual way, counting the net vorticity there by summing the in-plane angular changes around the cell and normalizing by 2π :

$$q = \frac{1}{2\pi} \sum_{\text{edge bonds}} \Delta\phi_{\text{bond}}. \quad (12)$$

It is understood that each difference between two in-plane spin angles along one edge segment must be taken on the primary branch: $-\pi/2 < \Delta\phi_{\text{bond}} < \pi/2$. Then q within a cell is forced to be an integer. In practice, the possible outcomes for q are 0 and ± 1 , as higher charged vortices are unstable within a single cell of the lattice, and never occur in Monte Carlo simulations.

Additionally, the search for vorticity can also be performed easily around the quartet of unit cells that surrounds an individual vacancy. A vacancy is surrounded automatically by eight occupied sites, connected by eight bonds (under our assumption of repulsive vacancies). Then again Eq. (12) can be applied to determine the total vorticity within these four cells nearest the vacancy,

$T = 0.850 \text{ e} = 1.12830 \text{ m} = 0.03405 \text{ } 0.01464 \text{ } -0.01900$

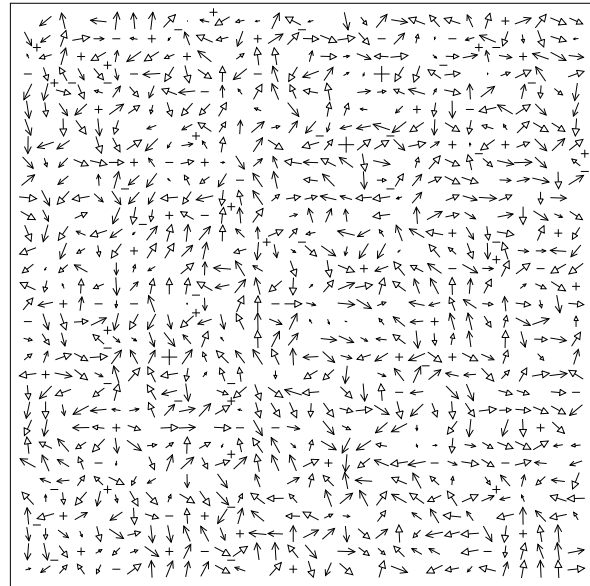


FIG. 4: A spin configuration from MC simulations for $L = 32$, $\lambda = 0$, $\rho_{\text{vac}} = 0.16$, at $T = 0.85J$, with vortices indicated by \pm signs. The projections of the xy spin components are shown as arrows, with line and triangular heads indicating positive/negative z spin components. The three larger plus signs are vortices of charge $q = +2$ centered on vacancies. Many vortices have formed centered on vacancies.

summing over the in-plane angular changes in all eight bonds. Now it is seen that the result for q can take the additional possible values $q = \pm 2$, i.e., *doubly charged vortices* are found to be stable entities when localized on the vacancies, but never are found to occur separated from a vacancy.

An example of a state with doubly charged vortices is given in Fig. 4, produced in the MC simulations with $L = 32$, $\lambda = 0$, $\rho_{\text{vac}} = 0.16$, at $T = 0.85J$, well above the critical temperature ($T_c \approx 0.478J$) for this vacancy concentration. The locations of the $q = 2$ vortices are indicated by the larger plus signs; two near the top-center and one in the lower-left section of the system. Other singly charged vortices are indicated by the smaller \pm signs. One can also note the considerable number of vortices (of any charge) that form exactly centered on the vacancies.

For a state in which there are n_1 singly charged vortices (q either $+1$ or -1) and n_2 doubly charged vortices (q either $+2$ or -2), the total absolute vorticity density was defined relative to the occupied spin sites, and giving a double weight to the double charges,

$$\rho = \frac{\sum_i |q_i|}{N} = \frac{n_1 + 2n_2}{N}. \quad (13)$$

Additionally, the vorticity fraction f_{dbl} that corresponds

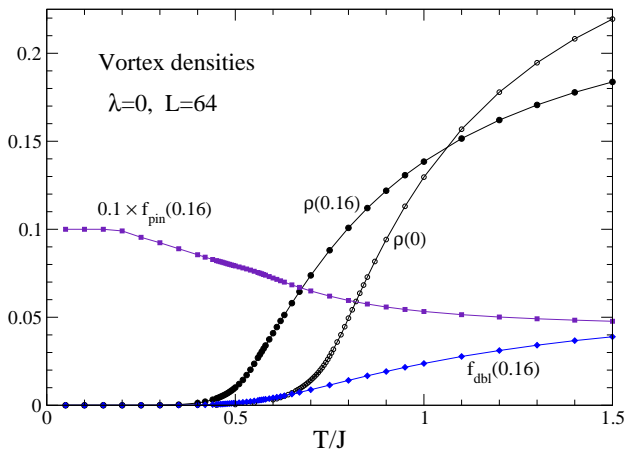


FIG. 5: Thermally induced vorticity density for the uniform XY model [$\rho(0)$] and at 16% vacancy density [$\rho(0.16)$]. Also displayed are the vorticity fraction pinned on vacancies [f_{pin}] and the fraction with doubled charges [f_{dbl}], both when $\rho_{\text{vac}} = 0.16$.

to doubly-charged vortices was tracked,

$$f_{\text{dbl}} = \frac{2n_2}{n_1 + 2n_2}. \quad (14)$$

Indeed, both the $q = \pm 1$ and $q = \pm 2$ vortices are commonly found centered on the vacancies. Therefore, we also calculated the fraction f_{pin} of the total absolute vorticity that is found centered on vacancies, or, pinned on the vacancies:

$$f_{\text{pin}} = \frac{\sum_i |q_i^{(\text{pinned})}|}{\sum_i |q_i|}, \quad (15)$$

where the sum in the denominator is over all vortices found in the system. As already mentioned above, the doubly charged vortices are always found pinned on the vacancies. Furthermore, at low temperatures with very low vortex density, essentially all vortices nucleate on vacancies.

Typical results for these various vorticity densities in the XY model at $L = 64$ are shown in Fig. 5. Considering the curves for 16% vacancy concentration, it is significant that for temperatures near T_c , the pinned vorticity fraction is around 75%. This is reasonable, because pinned $q = 1$ vortices have considerably lower energy than free ones and therefore will dominate at the lower temperatures. On the other hand, doubly-charged vorticity does not appear with significant population until well into the high-temperature phase, when it composes up to several percent of the total vorticity in the system.

E. Variations with λ

The previous sections presented vacancy effects in the XY model, $\lambda = 0$. MC simulations were also carried

TABLE I: Dependence of critical temperature $T_c(\rho_{\text{vac}})$ on anisotropy constant λ , for the pure model ($\rho_{\text{vac}} = 0$) and at $\rho_{\text{vac}} = 0.16$, obtained by the scaling of in-plane susceptibility.

λ	$T_c(0)/J$	$T_c(0.16)/J$
0.0	0.699 ± 0.001	0.478 ± 0.001
0.7	0.673 ± 0.001	0.454 ± 0.001
0.9545	0.608 ± 0.001	0.404 ± 0.001

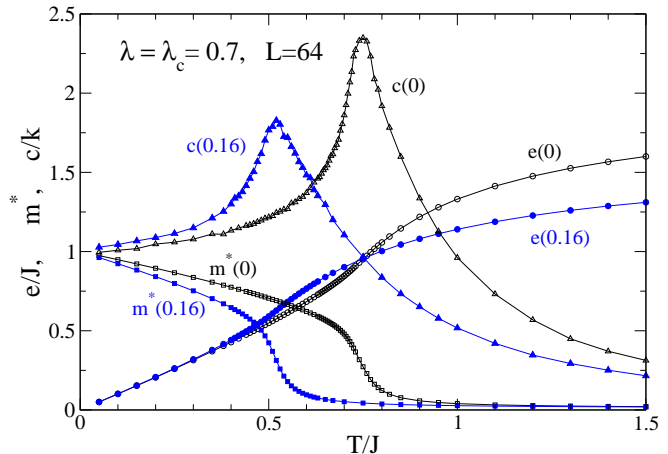


FIG. 6: For the model with edge $L = 64$, at the vortex-in-plaquette critical anisotropy, the internal energy, absolute magnetization, and specific heat per spin for the uniform system and with 16% vacancy density.

out at two nonzero values of the anisotropy parameter: 1) the vortex-in-plaquette critical anisotropy ($\lambda_c = 0.70$) and 2) the vortex-on-vacancy critical anisotropy ($\lambda_{\text{cv}} = 0.9545$). At λ_c large out-of-plane magnetization fluctuations might be expected if free vortices were dominating the dynamics. At λ_{cv} large out-of-plane magnetization fluctuations might be expected if vortices pinned on vacancies were dominating the dynamics.

At these nonzero λ , the effects due to vacancies are similar to those found at $\lambda = 0$: reduction of T_c , significant fraction of pinned vorticity in the low-temperature phase, and appearance of doubly charged vorticity in the high-temperature phase.

These limited results for T_c as determined by scaling of χ are summarized in Table I. At 16% vacancy concentration, the general dependence of T_c on λ mimics that found for the pure model; T_c changes very little until λ becomes very close to 1.

The per-spin energy, absolute in-plane magnetization, and specific heat at $\lambda = \lambda_c$ are shown in Fig. 6, where a mildly different result is seen compared to the XY model.

At λ_{cv} , stronger effects are found, as seen in Fig. 7. The transition temperature is reduced to $T_c/J \approx 0.404$ when 16% vacancies are present, Fig. 8, compared to $T_c/J \approx 0.608$ for the pure system. The vorticity density results are shown in Fig. 9, and mimic those found

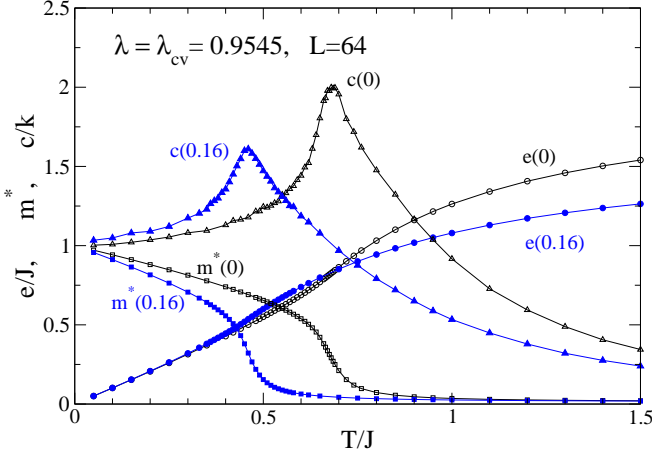


FIG. 7: For the model with edge $L = 64$, at the vortex-on-vacancy critical anisotropy, the internal energy, absolute magnetization and specific heat per spin for the uniform system and with 16% vacancy density.

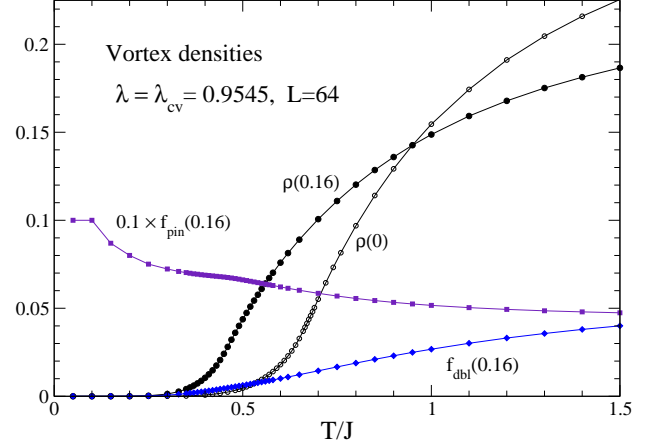


FIG. 9: Thermally induced vorticity density $[\rho(0)]$ at the vortex-on-vacancy critical anisotropy with 16% vacancy density $[\rho(0.16)]$. Also displayed are the vorticity fraction pinned on vacancies $[f_{\text{pin}}]$ and the fraction due to double charges $[f_{\text{dbl}}]$, at 16% vacancy density.

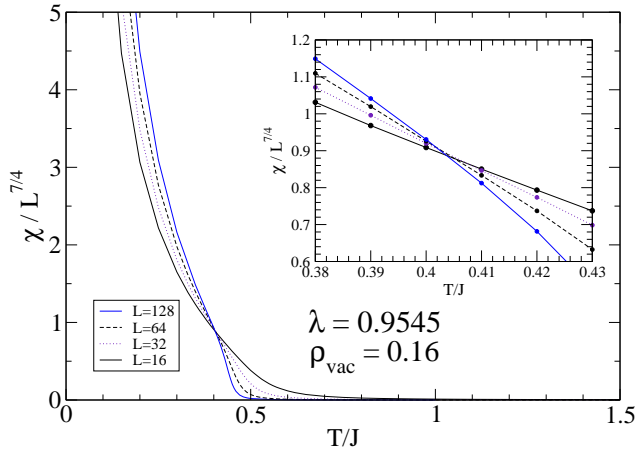


FIG. 8: Application of the finite-size scaling of in-plane susceptibility to estimate $T_c/J \approx 0.404$ (common crossing point of the data) at 16% vacancy density at the vortex-on-vacancy critical anisotropy.

for the XY model. Comparing the results at the different anisotropies, there is no sudden change in the vacancy effects, as far as can be seen from these limited data. The out-of-plane fluctuations vs. T for these nonzero λ do not exhibit any particularly significant features due to the presence of vacancies. Generally, in the low-temperature phase, χ^{zz} increases with vacancy density, but even more so with increasing λ , as summarized in Fig. 10. It is clear that the out-of-plane fluctuations are aided by the presence of vacancies, but from the limited data here, no significant conclusion about the role of pinned vortices vs. free vortices can be drawn.

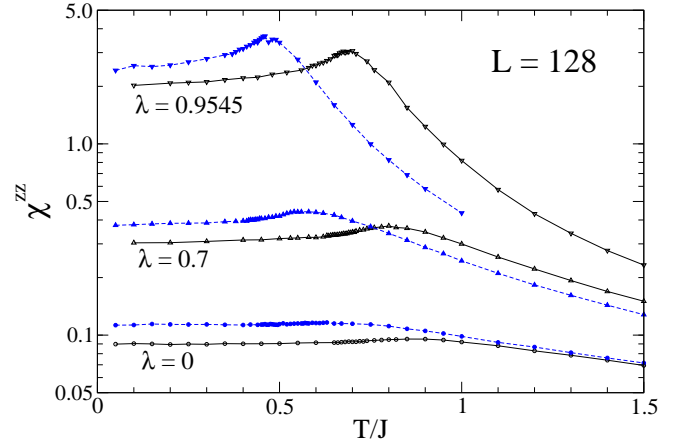


FIG. 10: Out-of-plane susceptibilities χ^{zz} vs. temperature for $L = 128$, at the three anisotropies studied. The lower curves at low T (open symbols) correspond to $\rho_{\text{vac}} = 0$, the upper curves (solid symbols) correspond to $\rho_{\text{vac}} = 0.16$. Unlike χ^{xx} or χ^{yy} , there is only a very weak dependence of χ^{zz} on L , mostly in the high-temperature phase.

IV. DOUBLY-CHARGED VORTEX CONFIGURATIONS FROM SPIN RELAXATIONS

Having seen the appearance, in general, of doubly charged vorticity localized on the vacancies, it is important to consider the basic analysis of their energetics. Clearly, in continuum theory, the static vortex energy (dependent on an integral of the form $J \int d^2x |\nabla\phi|^2 \approx J\pi q^2 \ln(R/a)$) is proportional to the squared charge. Therefore, one expects that the doubly-charged vortices, even when pinned on vacancies, should have considerably higher energy than singly-charged vortices (either pinned or free). Apparently, the absence of a spin at the center

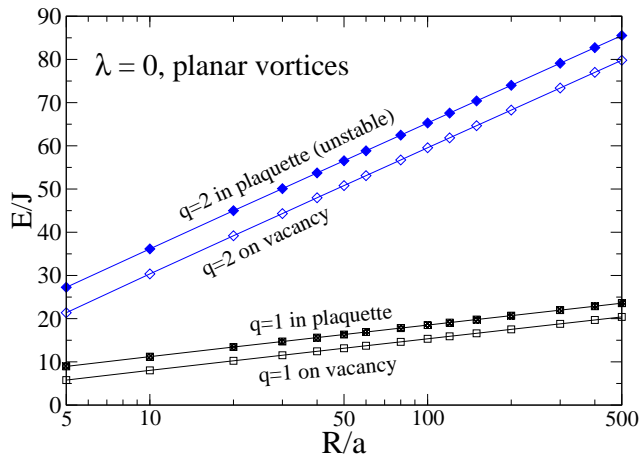


FIG. 11: Various total system energies with a vortex present versus system radius R .

of the $q = 2$ vortex, and the missing four interior bonds, significantly reduces the energy and allows for stability.

Following the procedure in Ref. 7, some doubly-charged vortex configurations were investigated numerically for their stability as a function of the anisotropy. For simplicity, a circular system of radius R , with sites defined on a square lattice, was used. The vacant site was placed exactly at the center of the circular system. Free boundary conditions applied at the edge of the system. The initial in-plane spin angles were set to that for a charge q vortex centered at position (x_v, y_v) ,

$$\phi(x, y) = q \tan^{-1} \left(\frac{y - y_v}{x - x_v} \right) + \phi_0. \quad (16)$$

For a $q = \pm 2$ vortex at the center of the system, a convenient way to implement this expression on the xy spin components for arbitrary constant $\phi_0 = 0$, without using trigonometric functions is

$$S^x(x, y) = \frac{x^2 - y^2}{x^2 + y^2}, \quad S^y(x, y) = \frac{\pm 2xy}{x^2 + y^2}, \quad (17)$$

the \pm signs producing vortex/antivortex configurations.

In order to test the in-plane to out-of-plane stability, all out-of-plane spin components were given small initial values $S^z = 0.001$, thereby biasing the spin configuration possibly to go out-of-plane along the positive z -axis. After this small perturbation, all spins were normalized to unit length. The spin configuration was relaxed iteratively by setting each spin to point along the direction of the effective field due to its neighbors, keeping the spin length fixed at unity. This leads eventually to a final configuration that is a local energy minimum of the Hamiltonian, i.e., some form of stable configuration evolved from the original state, in some case with vorticity still present, and in other cases, no net vorticity.

A. $q = 2$ vortex relaxation for XY model ($\lambda = 0$)

The first numerical relaxations were applied for the XY limit, $\lambda = 0$, to get the general idea of the energy compared to that for $q = 1$ vortices. Typically, the energy found at $\lambda = 0$ should be expected to apply rather accurately to larger values of λ , as long as the vortex remains in the planar configuration. These relaxations were performed for systems with radius ranging from $R = 5a$ to $R = 500a$, as the energy is expected to have a logarithmic dependence on R . The energy results E_{vv} for a $q = 2$ vortex centered on the vacancy are shown in Fig. 11, and compared with similar results for $q = 1$ vortices. Additionally, the vortex energies E_{vp} are shown when centered in a plaquette. For $q = 1$, this energy was found by relaxation to a stable vortex state, whereas, for $q = 2$, expression (16) was used to set the vortex centered in the plaquette, after which the energy was directly evaluated. This latter configuration for $q = 2$ is unstable, but was used for estimation of the vortex-on-vacancy binding energy, see below.

Inspection of Fig. 11 shows that, as expected, the doubly-charged vortices have considerably higher energy compared to singly charged, and furthermore, there is a nearly constant energy gap between the vortex-in-plaquette and vortex-on-vacancy states. Each data set fits extremely well to a logarithmic dependence on R in the form $E = A + B \ln(R/a)$. For $q = 1$, both curves have slope parameter $B_1 \approx 3.17JS^2$. For $q = 2$, both curves have slope parameter $B_2 \approx 12.7JS^2$, a value very close to four times as large as that for $q = 1$, as might be expected. The extra energy requirement for the $q = 2$ vortices clearly leads to a restriction on their thermal population compared to $q = 1$ vortices. In all cases shown, the final spin configuration was found to be completely in-plane (all $S^z = 0$).

The difference between the vortex-on-vacancy and vortex-in-plaquette energies can be taken to define an energy for binding or pinning the vortex on the vacancy,

$$\Delta E_q = E_{q,vp} - E_{q,vv}. \quad (18)$$

Using the results shown, the binding energy for a $q = 1$ vortex-on-vacancy is $\Delta E_1 \approx 3.177JS^2$, using the asymptotic value as $R \rightarrow \infty$. For doubly charged vortices, the binding energy is moderately higher, $\Delta E_2 \approx 5.73JS^2$, in contrast to the considerably higher creation energy for $q = 2$ vortices compared to $q = 1$ vortices. This result, however, must be taken with caution, since there is no actual stable $q = 2$ vortex free from a vacancy.

An alternative view of the $q = 2$ vortex-on-vacancy energy would be to compare it to twice the energy of a system with a single $q = 1$ vortex centered in a plaquette, ($2E_{1vp}$), because that is a stable state of the same total vorticity. However, the energy of the two $q = 1$ vortices, in their own isolated systems, is always considerably less than that of a single $q = 2$ vortex. This is because $2E_{1vp}$ does not include the interaction potential

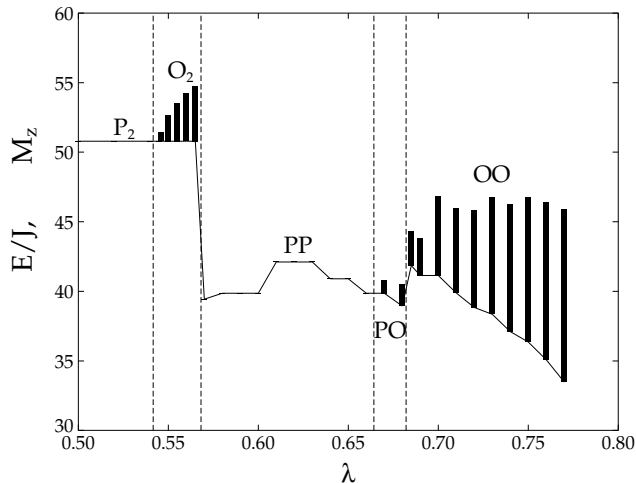


FIG. 12: After relaxation of a $q = 2$ vortex initially centered on an isolated vacancy in a circular system of radius $R = 50$, the total system energy (solid curve) is shown as a function of the anisotropy constant λ . The vertical bars indicate the net out-of-plane magnetization of the relaxed configuration, on the same numerical scale.

that would be present between two $q = 1$ vortices within the same system, which increases with the logarithm of their separation. Thus it is not a good reference number for estimation of the $q = 2$ binding energy on a vacancy.

B. Anisotropy dependence of $q = 2$ vortex relaxation

A preliminary analysis of the stability of a doubly-charged vortex can be performed by looking at the dependence of the relaxed configuration on the anisotropy parameter $\lambda \geq 0$. It might be expected that a $q = 2$ vortex could take on nonzero out-of-plane components when λ becomes adequately close to 1, i.e., at weak easy-plane anisotropy, in a manner similar to the out-of-plane crossover for $q = 1$ vortices. The critical anisotropy could be expected to be different than the value $\lambda_{cv} \approx 0.9545$ for pinned $q = 1$ vortices. Therefore, a limited number of numerical experiments were realized on a circular system of radius $R = 50a$ for various values of λ above zero. Again, the initial condition was a $q = 2$ vortex centered on the vacancy at the center of the system, with small positive out-of-plane components ($S^z = 0.001$) at all sites.

Certain aspects of these results are summarized in Fig. 12, where the energy of the state obtained after the relaxation is plotted versus the anisotropy parameter λ that was used. There are several types of results, depending on the range of λ being considered.

For the whole range $0 \leq \lambda \lesssim 0.545$ (region P_2), the isolated $q = 2$ vortex remains in a stable planar configuration on the vacancy, with no out-of-plane mag-

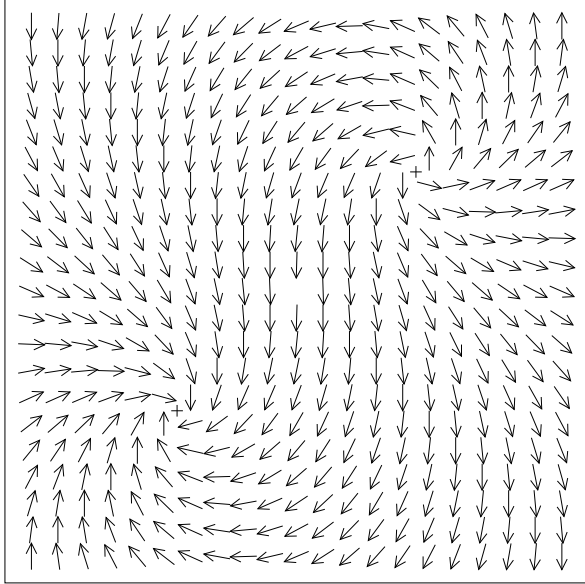
netization, and relatively high energy. For the narrow range $0.545 \lesssim \lambda \lesssim 0.57$ (region O_2), the $q = 2$ vortex remains stable on the vacancy, but develops nonzero out-of-plane magnetization, with an insignificant reduction in energy. The net out-of-plane magnetization of the relaxed state is indicated in Fig. 12 by the bars extending above the energy curve. Total M_z grows until λ reaches about 0.57, at which point the $q = 2$ vorticity concentrated on the vacancy becomes unstable, and breaks into one $q = 1$ in-plane vortex on the vacancy, and a nearby free $q = 1$ in-plane vortex. This situation holds for $0.57 \lesssim \lambda \lesssim 0.66$ (region PP); the configuration has zero out-of-plane magnetization once again, and lower energy than that for the $q = 2$ vortex pinned on a vacancy. As λ increases within this range, the free vortex progressively moves farther from the vacancy.

When λ ranges from about 0.67 to 0.68 (region PO), the free vortex starts to develop a nonzero positive out-of-plane component, while the pinned vortex remains planar. Finally, at $\lambda \approx 0.685$ and above (region OO), the relaxed configuration consists of two $q = 1$ positively polarized out-of-plane vortices centered symmetrically on opposite sides of the vacancy. For example, the relaxed configuration obtained for $\lambda = 0.7$ is shown in Fig. 13. As λ increases, the separation of the pair increases at the same time that their out-of-plane component increases, while the energy decreases. Eventually, the separation surpasses the diameter of the system, and the vorticity escapes out the boundary, leaving a final configuration with uniform magnetization and zero energy. This occurred for $\lambda \gtrsim 0.77$ in the system of radius $R = 50$.

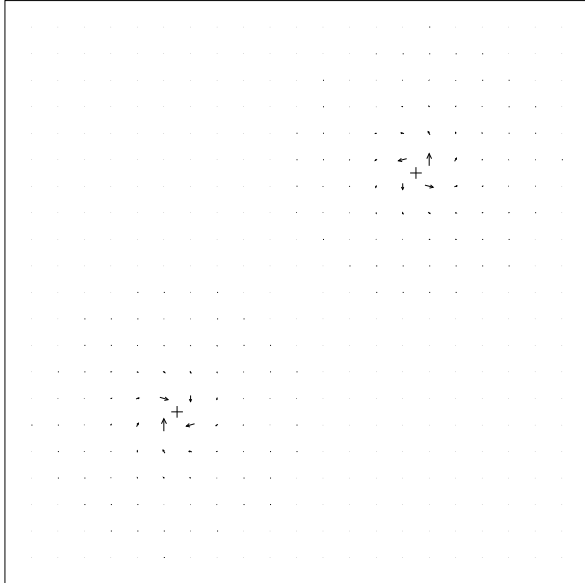
It is apparent that a localized $q = 2$ vorticity has severely limited stability, compared to $q = 1$ vortices. The $q = 2$ vorticity even tends to grow out-of-plane components as a way to enhance its stability, but this has a very limited range of utility (region O_2). Once the vorticity splits into individual $q = 1$ vortices, they are seen to influence each other, probably via an interaction with the vacancy. This is apparent because out-of-plane components begin forming for λ below the critical anisotropy parameter λ_c relevant for vortices far from vacancies. Furthermore, the pairs of out-of-plane $q = 1$ vortices in region OO appear to repel each other, while at the same time being attracted to the vacancy, which would lead to a mechanically stabilized configuration. Inspection of the spin configurations in region OO (as in Fig. 13) shows spin components of one vortex to be completely symmetrical to the spin components in the other vortex, when reflected across the center of the system.

V. CONCLUSIONS

In the Monte Carlo and spin dynamics calculations presented here for a 2D easy-plane anisotropic Heisenberg model, the presence of vacancies has been seen to affect the details of the BKT transition and the types of vorticity present.



(a)

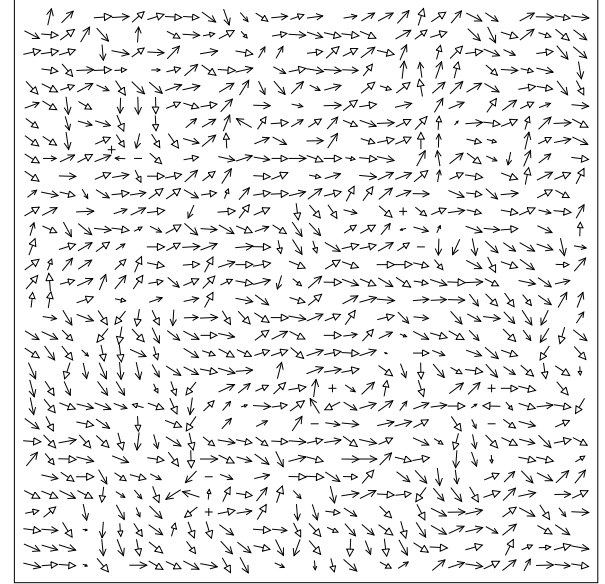


(b)

FIG. 13: Final state of relaxation of a $q = 2$ vortex initially centered on an isolated vacancy in a circular system of radius $R = 50$ with $\lambda = 0.7$ (only the central region of system is shown). Part (a) shows the projection of xy spin components on the plane, as explained in Fig. 4. In part (b) the lengths of the arrows are equal to the z spin components, while the directions are still given by the xy projections.

As seen in the planar rotator model, T_c is lowered by the presence of vacancies. This naturally results because the disorder in the transition becomes dominated by the generation of vortices pinned on the vacancies. When formed centered on vacancies, the vortex energy is significantly lower than that for vortices centered in plaquettes.

$T= 0.480$ $e= 0.53481$ $m= 0.65824$ -0.10391 0.00895



Sys 1/1, 860 Spins

$v=10$, $pin=9$, $dbl=0$

FIG. 14: A spin configuration for $L = 32$, $\lambda = 0$, $\rho_{vac} = 0.16$, at $T \approx T_c \approx 0.48J$, where 9 out of the 10 vortices present have formed on vacancies.

Indeed, $q = 1$ vortices pinned on vacancies in a square lattice, have a formation energy of about $3.17JS^2$ less than when centered in plaquettes, while the transition temperature corresponds to an energy less than $1JS^2$. Thus, at temperatures near and below T_c , the small amount of vorticity that is present is predominantly pinned on vacancies, such as in Fig. 14. These pinned vortices are initiating and controlling the transition. The vacancies are the nucleation sites for the spin disordering. On the other hand, vacancies reduce the rate at which total vorticity density rises in the high-temperature phase (Figs. 5, 9).

At larger anisotropy parameter λ_c , it is known that the vortex-on-vacancy energy is much closer to the vortex-in-plaquette energy.⁷ For example, at $\lambda = 0.99$, the difference in these energies is only $0.23JS^2$. Then one might expect a lesser dominance of pinned vorticity, however, that does not appear to be the case at $\lambda = \lambda_{cv}$. There is no substantial qualitative change in the fraction of pinned vorticity when compared to the XY model. Qualitatively speaking, the details of the BKT transition at higher λ , with vacancies, are not significantly different than those found for the XY model.

The presence of vacancies leads to a new effect, namely, the generation of doubly-charged vorticity that is stable when centered on vacancies. In thermal equilibrium, this effect apparently occurs regardless of the easy-plane anisotropy strength. In general, these would be thermodynamically prohibited, due to their larger energy, based on the usual dependence of vortex creation energy on charge squared. They still have significantly higher en-

ergy than singly charged vortices centered on vacancies, however, the missing bonds in the core region help to reduce their total energy compared to what they would have if centered in a plaquette.

A spin-relaxation energy minimization shows that an individual doubly-charged vortex centered on a vacancy in a circular system may be stable only for a limited range of anisotropy constant. The $q = 2$ vortex-on-vacancy stays stable and planar for $0 \leq \lambda \lesssim 0.545$. In a very narrow range, $0.545 \lesssim \lambda \lesssim 0.57$, the $q = 2$ vortex-on-vacancy still remains stable, but with a small out-of-plane component. For $\lambda \gtrsim 0.57$, it does not appear to be stable, but instead breaks apart into two $q = 1$ vortices that repel each other while being attracted to the vacancy. One might define a lower critical anisotropy $\lambda_{cv,1} \approx 0.545$ for the in-plane to out-of-plane $q = 2$ stability, and an upper critical anisotropy $\lambda_{cv,2} \approx 0.57$ for the breakdown into lower charged vorticities. In contrast, there is no choice of anisotropy constant that stabilizes a $q = 2$ vortex in the center of a plaquette.

These results are intriguing, because even though they show a limited range of stability for doubly-charged vorticity, nevertheless, these excitations appear in the MC

simulations at $\lambda = 0.7$ and $\lambda = 0.9545$, above the critical anisotropy parameters. Of course, one could always search groups of four plaquettes in the pure model also to find localized vorticity of double charge (two $q = 1$ vortices in neighboring plaquettes), although it would appear very rarely, due to the mutual repulsion of the vortices. The difference here, is that the presence of a vacancy attracts vorticity and certainly enhances the chances to find doubled vorticity within the area of four neighboring plaquettes. In addition, the spin relaxations show that the doubly charged vortex can be a static object, which can never be expected for $q = 1$ vortices in neighboring fully occupied plaquettes.

Acknowledgments

The author is very grateful for the hospitality of the Universidade Federal de Viçosa, Brazil, where this work was completed under support from FAPEMIG, and for many helpful discussions there with A. R. Pereira.

* Electronic address: wysin@phys.ksu.edu; URL: <http://www.phys.ksu.edu/~wysin>

† Permanent address: Department of Physics, Kansas State University, Manhattan, KS 66506-2601

¹ V. L. Berezinskiĭ, Sov. Phys. JETP **32**, 493 (1970).

² V. L. Berezinskiĭ, Sov. Phys. JETP **34**, 610 (1972).

³ J. M. Kosterlitz and D. J. Thouless, J. Phys. **C 6**, 1181 (1973).

⁴ K. Subbaraman, C. E. Zaspel, and J. E. Drumheller, Phys. Rev. Lett. **80**, 2201 (1998).

⁵ C. E. Zaspel, J. E. Drumheller, and K. Subbaraman, Phys. Stat. Sol. (a) **189**, 1029 (2002).

⁶ C. E. Zaspel, C. M. McKennan, and S. R. Snaric, Phys. Rev. B **53**, 11317 (1996).

⁷ G. M. Wysin, Phys. Rev. B **68**, 184411 (2003).

⁸ A. R. Pereira, L. A. S. Mól, S. A. Leonel, P. Z. Coura, and B. V. Costa, Phys. Rev. B **68**, 132409 (2003).

⁹ F. M. Paula, A. R. Pereira, and L. A. S. Mól, Phys. Lett. **A 329**, 155 (2004).

¹⁰ L. A. S. Mól, A. R. Pereira, and A. S. T. Pires, Phys. Rev. B **66**, 052415 (2002).

¹¹ S. A. Leonel, P. Z. Coura, A. R. Pereira, L. A. S. Mól, and B. V. Costa, Phys. Rev. B **67**, 104426 (2003).

¹² L. A. S. Mól, A. R. Pereira, and W. A. Moura-Melo, Phys. Rev. B **67**, 132403 (2003).

¹³ A. R. Pereira and A. S. T. Pires, J. Magn. Magn. Mater. **257**, 290 (2003).

¹⁴ B. Berche, A. I. Fariñas-Sánchez, Y. Holovatch, and R. P. V. Eur. Phys. J. **B 36**, 91 (2003).

¹⁵ L. M. Castro, A. S. T. Pires, and J. A. Plascak, J. Magn. Magn. Mater. **248**, 62 (2002).

¹⁶ S. Hikami and T. Tsuneto, Prog. Theor. Phys. **63**, 387

(1980).

¹⁷ S. Takeno and S. Homma, Prog. Theor. Phys. **64**, 1193 (1980).

¹⁸ S. Takeno and S. Homma, Prog. Theor. Phys. **65**, 172 (1980).

¹⁹ D. P. Landau, K. K. Mon, and H.-B. Schötler, eds., *Computer Simulation Studies in Condensed Matter Physics* (Springer-Verlag, Berlin, 1988).

²⁰ M. E. Gouvêa, G. M. Wysin, A. R. Bishop, and F. G. Mertens, Phys. Rev. B **39**, 11840 (1989).

²¹ G. M. Wysin, Phys. Rev. B **49**, 8780 (1994).

²² G. M. Wysin, Phys. Lett. **A 240**, 95 (1998).

²³ M. E. Gouvêa and G. M. Wysin, Phys. Rev. B **56**, 14192 (1997).

²⁴ C. Kawabata, M. Takeuchi, and A. R. Bishop, J. Magn. Magn. Mater. **54-57**, Pt.2, 871 (1986).

²⁵ C. Kawabata, M. Takeuchi, and A. R. Bishop, J. Stat. Phys. **43**, 869 (1986).

²⁶ G. M. Wysin and A. R. Bishop, Phys. Rev. **B 42**, 810 (1990).

²⁷ D. P. Landau, J. Magn. Magn. Mater. **200**, 231 (1999).

²⁸ H. G. Evertz and D. P. Landau, Phys. Rev. B **54**, 12302 (1996).

²⁹ U. Wolff, Nucl. Phys. B **300**, 501 (1988).

³⁰ U. Wolff, Phys. Rev. Lett. **62**, 361 (1989).

³¹ K. Binder, Z. Phys. B **43**, 119 (1981).

³² V. Privman, ed., *Finite Size Scaling and Numerical Simulation of Statistical Systems* (World Scientific Publishing, Singapore, 1990).

³³ A. Cuccoli, V. Tognetti, and R. Vaia, Phys. Rev. B **52**, 10221 (1995).